STAR-VP: Improving Long-term Viewport Prediction in 360° Videos via Space-aligned and Time-varying Fusion

Baoqi Gao
State Key Laboratory of Networking and Switching Technology, Beijing University of Posts and Telecommunications
Beijing, China
E-BYTE Technology Co., Ltd.
Beijing, China
gaobaoqi@bupt.edu.cn

Daoxu Sheng
State Key Laboratory of Networking and Switching Technology, Beijing University of Posts and Telecommunications
Beijing, China
E-BYTE Technology Co., Ltd.
Beijing, China
shengdx@bupt.edu.cn

Lei Zhang
China Unicom Network Communications Co., Ltd.
Beijing, China
zhangl83@chinaunicom.cn

Qi Qi*
State Key Laboratory of Networking and Switching Technology, Beijing University of Posts and Telecommunications
Beijing, China
qiqi8266@bupt.edu.cn

Bo He
State Key Laboratory of Networking and Switching Technology, Beijing University of Posts and Telecommunications
Beijing, China
hebo@bupt.edu.cn

Zirui Zhuang
State Key Laboratory of Networking and Switching Technology, Beijing University of Posts and Telecommunications
Beijing, China
zhuangzirui@bupt.edu.cn

Jingyu Wang*
State Key Laboratory of Networking and Switching Technology, Beijing University of Posts and Telecommunications
Beijing, China
wangjingyu@bupt.edu.cn

Abstract

Accurate long-term viewport prediction in tile-based 360° video adaptive streaming helps pre-download tiles for a further future, thus establishing a longer buffer to cope with network fluctuations. Long-term viewport motion is mainly influenced by Historical viewpoint Trajectory (HT) and Video Content information (VC). However, HT and VC are difficult to align in space due to their different modalities, and their relative importance in viewport prediction varies across prediction time steps. In this paper, we propose STAR-VP, a model that fuses HT and VC in a Space-aligned and Time-vARying manner for Viewport Prediction. Specifically, we first propose a novel saliency representation *salxyz* and a Spatial Attention Module to solve the spatial alignment of HT and VC. Then, we propose a two-stage fusion approach based on Transformer and gating mechanisms to capture their time-varying importance. Visualization of attention scores intuitively demonstrates STAR-VP's capability in space-aligned and time-varying fusion. Evaluation on three public datasets shows that STAR-VP achieves state-of-the-art accuracy for long-term (2-5s) viewport prediction without sacrificing short-term (<1s) prediction performance.

CCS Concepts

• **Information systems** → **Multimedia streaming**; • **Mathematics of computing** → *Time series analysis*; • **Computing methodologies** → Neural networks.

Keywords

viewport prediction, 360° video, Transformer network, multi-modal fusion, saliency map

*Corresponding author.

Permission to make digital or hard copies of all or part of this work for personal or classroom use is granted without fee provided that copies are not made or distributed for profit or commercial advantage and that copies bear this notice and the full citation on the first page. Copyrights for components of this work owned by others than the author(s) must be honored. Abstracting with credit is permitted. To copy otherwise, or republish, to post on servers or to redistribute to lists, requires prior specific permission and/or a fee. Request permissions from permissions@acm.org.
MM '24, October 28-November 1, 2024, Melbourne, VIC, Australia
© 2024 Copyright held by the owner/author(s). Publication rights licensed to ACM.
ACM ISBN 979-8-4007-0686-8/24/10
https://doi.org/10.1145/3664647.3681268

ACM Reference Format:
Baoqi Gao, Daoxu Sheng, Lei Zhang, Qi Qi, Bo He, Zirui Zhuang, and Jingyu Wang. 2024. STAR-VP: Improving Long-term Viewport Prediction in 360° Videos via Space-aligned and Time-varying Fusion. In *Proceedings of the 32nd ACM International Conference on Multimedia (MM '24), October 28-November 1, 2024, Melbourne, VIC, Australia.* ACM, New York, NY, USA, 9 pages. https://doi.org/10.1145/3664647.3681268

1 INTRODUCTION

360-degree videos capture the full surrounding environment, enabling viewers to freely change perspectives during playback for a more immersive and interactive viewing experience. The data rate of 360-degree video needs to be approximately six times higher than that of regular video to achieve a comparable angular resolution [1]. The increased data rate poses significant challenges for real-time streaming of 360-degree video over the internet. Therefore, tile-based adaptive streaming [35] has been proposed to stream only the tiles within the user's Field of View (FoV) at higher bitrates, thus reducing bandwidth and computing resource overhead. Nevertheless, the effectiveness of tile-based adaptive streaming relies heavily on the accuracy of viewport prediction. Accurate long-term viewport prediction helps pre-download tiles for a further future, establishing a longer buffer to cope with network fluctuations. Long-term viewport motion is mainly influenced by Historical viewpoint Trajectory (HT) and Video Content information (VC), thus requiring the fusion of these two types of information for prediction.

However, the fusion of HT and VC for viewport prediction faces two key challenges: 1) ***Spatial alignment.*** HT is represented as coordinate sequences, while commonly used VC information such as saliency map [25, 39, 42] and motion map [11, 12] is represented as image. This makes it difficult for the model to align the spatial positions represented by the viewpoint coordinates and the pixel positions in VC information. 2) ***Time-varying importance.*** The relative importance of HT and VC in viewpoint prediction varies across prediction time steps. Intuitively, in the short term, the viewpoint tends to continue its previous motion patterns due to inertia, thus HT is more important; whereas in the long term, the viewpoint tends to be attracted by saliency regions within the video content, thus VC is more important [30]. However, this time-varying pattern of relative importance can be very complex and cannot be described by simple rules.

The example in Fig. 1 further illustrates the necessity of considering the above two challenges. In the spatial dimension, User 1 and User 2's viewpoints are attracted by different salient regions due to their different positions, thus the viewport prediction model needs to align the spatial positions expressed in HT and VC. In the temporal dimension, User 1's viewpoint maintains its previous motion pattern in the short term due to inertia, until it is mainly attracted by salient regions in the video content in the long term. Therefore, the viewport prediction model needs to capture the time-varying importance of HT and VC.

In this paper, we propose STAR-VP, a model that fuses HT and VC in a Space-aligned and Time-vARying manner for Viewport Prediction. Specifically, to address the spatial alignment of HT and VC, we first propose a novel saliency representation *salxyz*, which represents a 2D grayscale saliency map as a collection of `(3D spatial coordinates + saliency value)` tuples, explicitly injecting spatial coordinate information into saliency information. Then, we design a Spatial Attention Module with a Transformer-like architecture to solve the spatial alignment problem in conjunction with *salxyz*. To address the time-varying importance of HT and VC, we propose a two-stage fusion approach. In the first fusion stage, we design a Temporal Attention Module with a Transformer-like architecture. This module enables the model to adaptively adjust the attention to HT and VC features at each prediction step. In the second fusion stage, we design a Gating Fusion Module to further fuse the prediction results of the short-term prediction module and the long-term prediction module, enabling the model to have superior long-term prediction performance without sacrificing short-term prediction performance.

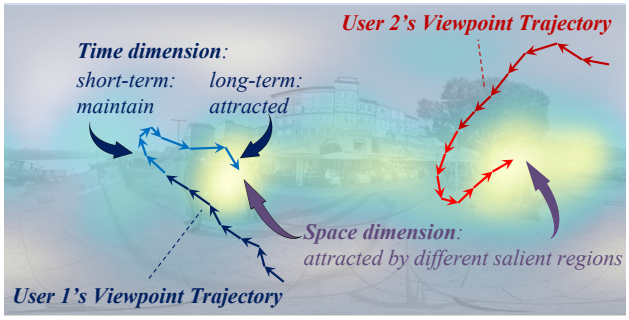

Figure 1: An example illustrating the necessity of considering the space alignment and time-varying importance of Historical viewpoint Trajectory (HT) and Video Content information (VC) in long-term viewport prediction.

To summary, our major contributions are as follows:

- We propose a novel saliency representation *salxyz*. It explicitly injects spatial coordinate information into saliency information to facilitate the spatial alignment of HT and VC.
- We propose STAR-VP, a long-term viewport prediction model. It achieves the spatial alignment of HT and VC through a Spatial Attention Module working with *salxyz*, and captures the time-varying importance of HT and VC through a two-stage fusion approach based on Transformer and gating mechanisms.
- We evaluate STAR-VP on three public datasets and show that it achieves state-of-the-art accuracy for long-term (2-5s) viewport prediction without sacrificing short-term (<1s) prediction performance.

2 RELATED WORK

2.1 Viewport Prediction in 360° Videos

To achieve more accurate prediction, most existing viewport prediction models consider not only the user's HT, but also auxiliary information such as saliency map [25, 31, 37, 40], motion map [11, 12], object trajectory [6, 19], and other users' HT [2, 5, 24]. In this paper, we mainly explore the fusion of HT and the most commonly used VC information, saliency map.

To address the spatial alignment of HT and VC, some works [25, 33] convert HT from coordinates into VC-like heatmap representations using Gaussian filtering. While this approach unifies the modalities of HT and VC, it increases computational and storage overheads. Moreover, the spatial position information expressed in 2D ERP images cannot well reflect the motion of the viewpoint on the 3D sphere.

Regarding the time-varying importance of HT and VC, most existing viewport prediction models [11, 25, 36] ignore it and simply

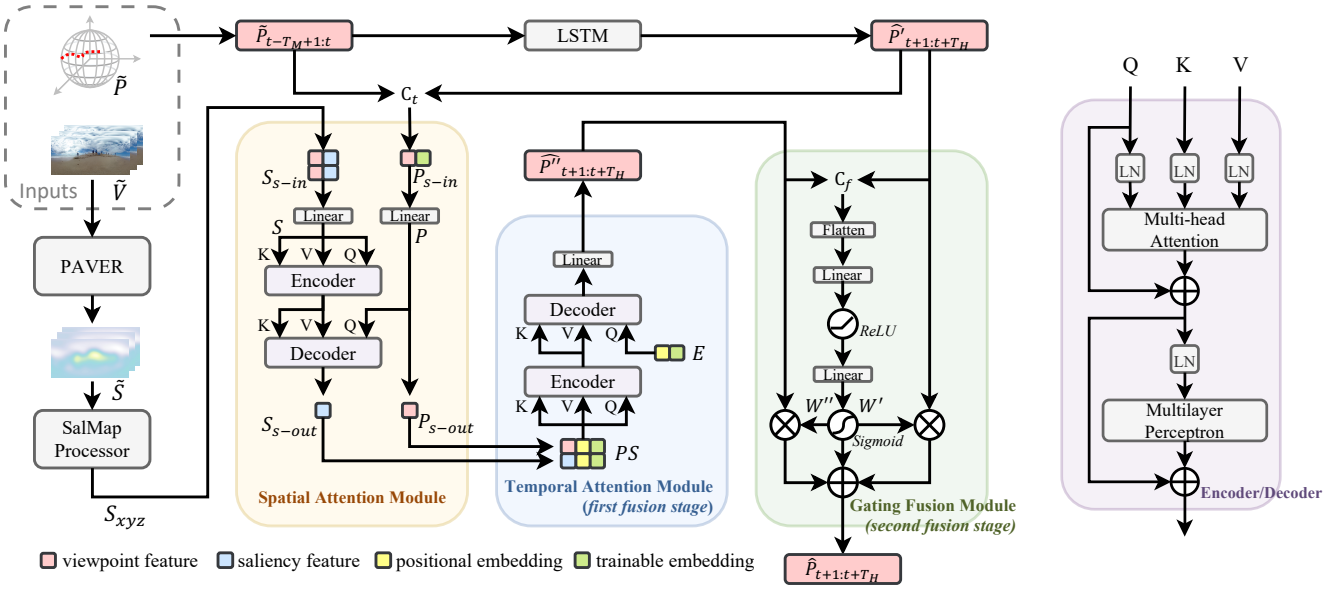

(a) STAR-VP Model Overview (b) Encoder/Decoder Structure

Figure 2: The architecture of STAR-VP. (a) shows the overall architecture of STAR-VP, including the SalMap Processor, LSTM module, Spatial Attention Module, Temporal Attention Module, and Gating Fusion Module. (b) shows the details of the Encoder/Decoder in the Spatial Attention Module and the Temporal Attention Module. The Encoder and Decoder have the same architecture but are based on self-attention and cross-attention, respectively. $C_f(\cdot)$ and $C_t(\cdot)$ denote concatenating vectors along the feature dimension and the temporal dimension, respectively. $\otimes$ and $\oplus$ denote element-wise multiplication and addition, respectively. LN denotes Layer Normalization.

concatenate HT and VC along the feature dimension. TRACK [30] uses three LSTM modules to separately process HT, VC, and their concatenated features, aiming to dynamically balance HT and VC across prediction time steps. However, due to the inherent inability of LSTMs to model complex and long-term dependencies, the TRACK model has limitations in capturing complex time-varying patterns of relative importance between HT and VC. HeMoG [29] is a white-box model built on physics of rotational motion and gravitation, achieving higher interpretability. However, its performance is sensitive to manually-tuned parameters. MFTR [41] uses three Transformer encoders [32] to separately process HT, VC, and their concatenated features. Compared to TRACK, MFTR more effectively learns the time-varying importance of HT and VC. However, MFTR still only adaptively selects HT and VC with time-varying patterns at the feature level, making it difficult to avoid sacrificing short-term prediction performance while improving long-term prediction performance.

2.2 Transformer and Gating Mechanisms

Transformer [32] was initially known for its excellent performance in natural language processing tasks such as machine translation. It aggregates information across the entire sequence with adaptive weights through attention mechanisms, capturing long-term dependencies in a parallel manner. In recent years, models based on the Transformer architecture have shown excellent performance not only in natural language processing tasks [9, 16, 27] but also in various visual tasks [3, 10, 20, 21] and multimodal tasks [17, 18, 22]. Since the fusion of HT and VC involves time series and multimodal data, it is suitable to use Transformer-based models for processing.

The application of gating mechanisms in neural networks can be traced back to the LSTM model [14]. LSTM uses three gating units to control the flow of information to better capture long-term dependencies. Since then, gating mechanisms have been widely used in various deep learning models [7, 26, 44] to better focus on important information and suppress irrelevant information.

3 METHOD

3.1 Overview

The overall architecture of STAR-VP is depicted in Fig. 2. STAR-VP predicts the viewpoint positions for the future T_H time steps($\widehat{P}$), given the viewpoint positions from the past T_M time steps ($\widetilde{P}$) and the video frames spanning both the past T_M and the future T_H time steps ($\widetilde{V}$). Each viewpoint position is represented as a 3D spatial coordinate on the unit sphere, and each video frame is represented as an image in Equi-Rectangular Projection (ERP) format.

STAR-VP mainly consists of five modules: SalMap Processor, LSTM module, Spatial Attention Module, Temporal Attention Module, and Gating Fusion Module. First, the original video frames $\widetilde{V}$ are converted into saliency maps $\widetilde{S}$ by PAVER [38], a model specifically designed for saliency detection in 360-degree videos. Then, the SalMap Processor converts $\widetilde{S}$ into the *salxyz* representation S_{xyz}. The LSTM module only uses the viewpoint positions from the past

T_M time steps to obtain predictions $\widehat{P'}$ with excellent short-term performance for the future T_H time steps. The Spatial Attention Module takes S_{xyz} and the concatenation of the historical viewpoint trajectory and the LSTM prediction results as input, and outputs the spatially aligned viewpoint position features P_{s-out} and saliency features S_{s-out}. The Temporal Attention Module is responsible for the first-stage fusion. It takes P_{s-out} and S_{s-out} as input, adaptively adjusts the focus on HT and VC features at each prediction time step through well-designed attention modules, and outputs predictions $\widehat{P''}$ with excellent long-term performance. The Gating Fusion Module is responsible for the second-stage fusion. It uses a gating mechanism to obtain the weights of $\widehat{P'}$ and $\widehat{P''}$ at each prediction time step, and outputs the final viewpoint prediction results $\widehat{P}$.

The following subsections will introduce the specific details of the five modules mentioned above and the internal Encoder/Decoder.

3.2 SalMap Processor

The SalMap Processor converts the original saliency map into a compact saliency representation with pixel coordinate information. Given the saliency map $\widetilde{S} \in \mathbb{R}^{(T_M+T_H)\times H\times W}$, the SalMap Processor represents each pixel's saliency information as (x, y, z, s), where (x, y, z) are the 3D coordinates of the pixel block center and s is the corresponding saliency value. The 3D coordinates (x, y, z) of the pixel block with index (i, j) are calculated as follows:

$$\begin{aligned}(x, y, z) &= (\cos\theta \cdot \sin\phi,\ \sin\theta \cdot \sin\phi,\ \cos\phi),\\ \theta &= \frac{2\pi}{W} \cdot (j + 0.5),\ \phi = \frac{\pi}{H} \cdot (i + 0.5),\end{aligned} \tag{1}$$

where H and W are the height and width of the saliency map respectively.

To reduce data redundancy, the SalMap Processor retains only the top tt points with maximum saliency, which are then sampled at rate sr. Finally, the SalMap Processor outputs $S_{xyz} \in \mathbb{R}^{(T_M+T_H)\times D_P\times 4}$, where $D_P = \lfloor tt \cdot sr \rfloor$.

3.3 LSTM Module

When watching 360-degree videos, users' viewpoint motion is relatively stable most of the time. Due to inertia, the future motion of the viewpoint, especially in the short term, is highly correlated with its historical trajectory. Therefore, we use LSTM, a lightweight and efficient temporal prediction model, to take only the viewpoint positions from the past T_M time steps as input and output predictions for the future T_H time steps in an autoregressive manner:

$$\widehat{P'}_{t+1:t+T_H} = \mathrm{LSTM}(\widetilde{P}_{t-T_M+1:t}), \tag{2}$$

where $\widetilde{P}_{t-T_M+1:t} \in \mathbb{R}^{T_M\times 3}$ is the viewpoint positions from the past T_M time steps, and $\widehat{P'} \in \mathbb{R}^{T_H\times 3}$ is the LSTM prediction results for the future T_H time steps. This prediction has excellent short-term performance. The specific details of the LSTM module are omitted here.

3.4 Spatial Attention Module

The Spatial Attention Module is based on a Transformer-like architecture. Compared to the original Transformer model, we have modified its positional encoding part and the structure and query input of its Decoder.

First, since both S_{xyz} and the viewpoint data already contain 3D spatial coordinate information, we modify the positional encoding in the original Transformer to trainable parameter embedding, aiming to unify the representations of the two modalities. The Spatial Attention Module takes S_{s-in} and P_{s-in} as input, where $S_{s-in} = S_{xyz} \in \mathbb{R}^{(T_M+T_H)\times D_P\times 4}$. The calculation formula of P_{s-in} is as follows:

$$P_{s-in} = \mathbf{C}_f(\mathbf{C}_t(\widetilde{P}_{t-T_M+1:t}, \widehat{P'}_{t+1:t+T_H}), TE) \in \mathbb{R}^{(T_M+T_H)\times 4}, \tag{3}$$

where $\mathbf{C}_f(\cdot)$ and $\mathbf{C}_t(\cdot)$ denote concatenating vectors along the feature dimension and the temporal dimension respectively, and $TE \in \mathbb{R}^{(T_M+T_H)\times 1}$ is a vector expanded from a 1×1 trainable parameter along the temporal dimension, used to transform P_{s-in} into a form similar to (x, y, z, s) of S_{s-in}, facilitating modality fusion and spatial alignment. Subsequently, two linear layers convert S_{s-in} and P_{s-in} into $S \in \mathbb{R}^{(T_M+T_H)\times D_P\times D_C}$ and $P \in \mathbb{R}^{(T_M+T_H)\times D_C}$, respectively.

Next, we unify the Decoder to have the same architecture as the Encoder, and use viewpoint features as the query input to the Decoder, fully utilizing the cross-attention mechanism to decode viewpoint-specific saliency features. The Encoder encodes S into S' using self-attention, with S serving as query, key, and value. The Decoder uses viewpoint position features P as query and S' as key and value, employing cross-attention to perceive the position information of viewpoint, giving higher attention to the saliency information near the viewpoint. Further details of the Encoder/Decoder are provided in Section 3.7.

3.5 Temporal Attention Module

Similar to the Spatial Attention Module, the Temporal Attention Module is also based on a Transformer-like architecture. Compared to the original Transformer model, we have modified its positional encoding part and the structure and query input of its Decoder.

First, we modify the positional encoding in the original Transformer to positional embedding and trainable modality-specific embedding. The Temporal Attention Module takes P_{s-out} and S_{s-out} as input, and outputs the composite vector $PS \in \mathbb{R}^{2(T_M+T_H)\times D_{PS}}$ as follows:

$$PS = \mathbf{C}_t(\mathbf{C}_f(P_{s-out}, PE, TE_P), \mathbf{C}_f(S_{s-out}, PE, TE_S)), \tag{4}$$

where $\mathbf{C}_f(\cdot)$ and $\mathbf{C}_t(\cdot)$ denote concatenating vectors along the feature dimension and the temporal dimension respectively, $PE \in \mathbb{R}^{(T_M+T_H)\times D_{PE}}$ is fixed 1D Fourier positional embeddings for a total of $T_M + T_H$ time steps, $TE_P \in \mathbb{R}^{(T_M+T_H)\times D_{TE}}$ and $TE_S \in \mathbb{R}^{(T_M+T_H)\times D_{TE}}$ are trainable modality-specific embeddings, and $D_{PS} = D_C + D_{PE} + D_{TE}$.

Next, we use the vector concatenated by positional embeddings and modality-specific embeddings as the query input to the Decoder, fully utilizing the cross-attention mechanism to decode the viewpoint information at each prediction step. The query embeddings $E \in \mathbb{R}^{T_H\times(D_{PE}+D_{TE})}$ are calculated as follows:

$$E = \mathbf{C}_f(PE_{t+1:t+T_H}, TE_{P,t+1:t+T_H}), \tag{5}$$

The Decoder in the Temporal Attention Module is also unified to have the same architecture as the Encoder. The Encoder encodes

PS into $PS^{'}$ using self-attention, with PS serving as query, key, and value. The Decoder uses E as query and $PS^{'}$ as key and value, employing cross-attention to perceive the specific temporal and modality information. This captures the time-varying importance of the viewpoint position features and saliency features. The Encoder/Decoder is introduced in detail in Section 3.7.

As the first fusion stage, the Temporal Attention Module adaptively adjusts the focus on HT and VC features at each prediction time step, outputting predictions $\widehat{P''} \in \mathbb{R}^{T_H \times 3}$ with excellent long-term performance.

3.6 Gating Fusion Module

As the second fusion stage, the Gating Fusion Module generates vectors $W^{'} \in \mathbb{R}^{T_H}$ and $W^{''} \in \mathbb{R}^{T_H}$ to control the weights of $\widehat{P'}$ and $\widehat{P''}$ at each prediction time step, and outputs the final viewpoint prediction results $\widehat{P} \in \mathbb{R}^{T_H \times 3}$:

$$\begin{aligned} &\widehat{P} = W^{'} \otimes \widehat{P'} \oplus W^{''} \otimes \widehat{P''},\ x = \text{Flatten}(\mathbf{C}_f(\widehat{P'}, \widehat{P''})), \\ &W^{'} = \sigma_s(W_s(\sigma_r(W_r x + b_r)) + b_s),\ W^{''} = 1 - W^{'} \end{aligned} \tag{6}$$

where $\otimes$ and $\oplus$ denote element-wise multiplication and addition respectively, $\mathbf{C}_f$ denotes concatenating vectors along the feature dimension, σ_r is the ReLU activation function, σ_s is the sigmoid activation function, $W_r \in \mathbb{R}^{D_G \times 6T_H}$, $b_1 \in \mathbb{R}^{D_G}$, $W_{g2} \in \mathbb{R}^{T_H \times D_G}$, and $b_2 \in \mathbb{R}^{T_H}$ are trainable parameters.

3.7 Encoder and Decoder

Inspired by the universal multimodal fusion architecture Perceiver IO [15], we unified the architecture of the Encoder and Decoder in the Spatial Attention Module and the Temporal Attention Module, and added some additional linear layers to adjust the feature dimensions of the vectors. The Encoder uses self-attention to extract deep features, while Decoder uses cross-attention to perceive current specific spatial/temporal information, achieving adaptive feature selection. The Encoder/Decoder consists of two components: the Multi-head Attention and the Multilayer Perceptron (MLP).

The Multi-head Attention component performs the following calculation given $Q_{in} \in \mathbb{R}^{n_q \times d_q}$, $K_{in} \in \mathbb{R}^{n_k \times d_k}$, and $V_{in} \in \mathbb{R}^{n_v \times d_v}$:

$$\begin{aligned} &\text{Attn}(Q_{in}, K_{in}, V_{in}) = \mathcal{L}_o(\text{softmax}(\frac{Q^{'}K^{'T}}{\sqrt{d_l}})V^{'}), \\ &Q^{'} = \mathcal{L}_q(Q_{in}),\ K^{'} = \mathcal{L}_k(K_{in}),\ V^{'} = \mathcal{L}_v(V_{in}), \end{aligned} \tag{7}$$

where $\mathcal{L}_{q,k,v}$ are linear layers mapping each input to a shared feature dimension d_l, and $\mathcal{L}_o$ is a linear layer projecting the output to a desired feature dimension. It is worth noting that all of these linear layers are applied convolutionally along the index dimension, and the batch and head dimensions have been excluded for clarity.

The MLP component consists of two linear layers with a GELU [13] nonlinearity applied after the first layer:

$$\text{MLP}(X_{in}) = \mathcal{L}_2(\text{GELU}(\mathcal{L}_1(X_{in}))) \tag{8}$$

The final output of the Encoder/Decoder is calculated as follows:

$$\begin{aligned} \text{Attention}(Q, K, V) &= \mathcal{A}(O_{attn}, \text{MLP}(\mathcal{N}(O_{attn}))), \\ O_{attn} &= \mathcal{A}(Q, \text{Attn}(\mathcal{N}(Q), \mathcal{N}(K), \mathcal{N}(V))), \end{aligned} \tag{9}$$

where $\mathcal{N}$ denotes layer normalization, and $\mathcal{A}$ denotes addition in residual connection.

4 EXPERIMENTS

STAR-VP is evaluated on a unified evaluation framework [28] for viewport prediction methods in 360-degree videos. The framework unifies five datasets into a common format (sampling period: 0.2s; viewpoint representation: 3D coordinates on the unit sphere) and summarizes current combination approaches of HT and VC, evaluating their performance.

4.1 Setup

4.1.1 Datasets. We evaluate STAR-VP on three datasets:
(1) *David_MMSys_18* [8] contains 19 20-second 360-degree videos in ERP format and head and eye tracking data from 57 participants watching the videos freely.
(2) *Nasrabadi_MMSys_19* [23] consists of 28 videos (60s) and viewport traces from 60 participants watching the videos. Each video is viewed by 30 participants.
(3) *Wu_MMSys_17* [34] includes head tracking data from 48 users watching 18 360-degree videos of 5 categories.

4.1.2 Competitors. Five models are implemented as competitors. Three of them only use HT:
(1) *linear-regression* predicts future viewpoint positions using a linear regression model.
(2) *deep-pos-only* is an LSTM-based encoder-decoder model. The encoder receives the historical viewpoint trajectory and generates an internal representation. The decoder receives the output of the encoder and progressively produces predictions over the target horizon, by re-injecting the previous prediction as input for the new prediction time-steps.
(3) *VPT360* [4] is a Transformer-based model. It only uses Transformer Encoder to process HT information for time series prediction.
The other two models use both HT and VC:
(4) *TRACK* [30] uses three LSTM modules to separately process HT, VC, and their concatenated features, aiming to dynamically balance HT and VC across prediction time steps.
(5) *MFTR* [41] is a complex multi-modal fusion Transformer-based model. However, its basic fusion framework for HT and VC is to use three Transformer-encoder-based modules to separately process HT, VC, and their concatenated features.

It is worth noting that the above comparison models basically cover all the fusion methods of HT and VC in the current viewport prediction models we know.

4.1.3 Performance Metrics. We use Orthodromic Distance (OD) [30] and Intersection over Union (IoU) [43] as the performance metrics.

The Orthodromic Distance between points $P1$ and $P2$ is calculated as follows:

$$OD(P_1, P_2) = \arccos(\vec{P_1} \cdot \vec{P_2}) \tag{10}$$

where P_1 and P_2 are two 3D coordinates on the unit sphere, and $\cdot$ is the dot product operation. When we use "3D spatial coordinates on the unit sphere" to represent the viewpoint position, the orthodromic distance actually represents the shortest spherical distance between the two viewpoints.

The Intersection over Union is an evaluation metric related to the specific tile partition method. We divide the ERP video frame into 9×16 tiles and set the user's field of view to 100°. If the angle between the center of the tile and the viewpoint is less than 50°, the tile is considered to be in the viewport, and its label is set to 1; otherwise, it is set to 0. Then, the Intersection over Union is computed on these labels as follows:

$$IoU = \frac{TP}{TT} \tag{11}$$

where TP represents *True Positive*, i.e., the intersection between prediction and ground-truth of tiles with label 1; TT represents *True Total*, i.e., the union of all tiles with label 1 in the prediction and in the ground-truth.

4.1.4 Saliency Map Generation and Processing. We use PAVER [38], a Vision Transformer-based model trained specifically for 360° video saliency detection, to compute the saliency map at each time step. The original 224×448 saliency maps are processed by the SalMap Processor module of STAR-VP to generate 128×4 compact saliency representation S_{xyz} with a top threshold (tt) of 20480 and sample rate (sr) of 1/160. In addition, for model size and memory considerations, the competitors use downsampled 64×128 saliency maps as the actual VC input. Even so, the data volume of saliency information actually used by STAR-VP is only 1/16 of that of other competitors.

4.1.5 Model Hyperparameters. The hyperparameters of all models are shown in Table 1. All models predict the next 5s (25 steps) of viewpoint positions based on the past 3s (15 steps).

Table 1: Hyperparameters of all models.

Symbol	Value	Description
D_{c^L}	256	Channel dimension of the hidden state in LSTM module.
D_{c^T}	256	Channel dimension of input of the Transformer encoder.
D_{PE}	129	Dimension of the positional embedding.
D_{TE}	127	Dimension of the trainable embedding.
D_G	128	Dimension of the hidden state in the Gating Fusion Module.
N_{layers^L}	2	Number of layers in LSTM module.
N_{layers^T}	2	Number of self-attention layers per block.
N_{blocks}	2	Number of blocks in the Transformer encoder.
N_{heads}	8	Number of heads in the multi-head attention layer.

Table 2: The average long-term prediction (2-5s) performance of viewport prediction models on three datasets. OD is Orthodromic Distance, and IoU is Intersection over Union.

	David_MMSys_18		Nasrabadi_MMSys_19		Wu_MMSys_17	
	OD ↓	IoU ↑	OD ↓	IoU ↑	OD ↓	IoU ↑
linear-regression	1.174	23.92%	0.962	35.41%	0.643	51.17%
deep-pos-only	1.145	26.35%	0.950	35.93%	0.623	52.37%
TRACK	1.123	25.05%	0.939	35.05%	0.613	51.12%
VPT360	1.127	26.00%	0.941	36.27%	0.624	52.04%
MFTR	1.064	27.98%	0.954	34.27%	0.599	52.02%
STAR-VP (ours)	**0.967**	**33.26%**	**0.862**	**39.84%**	**0.531**	**56.82%**

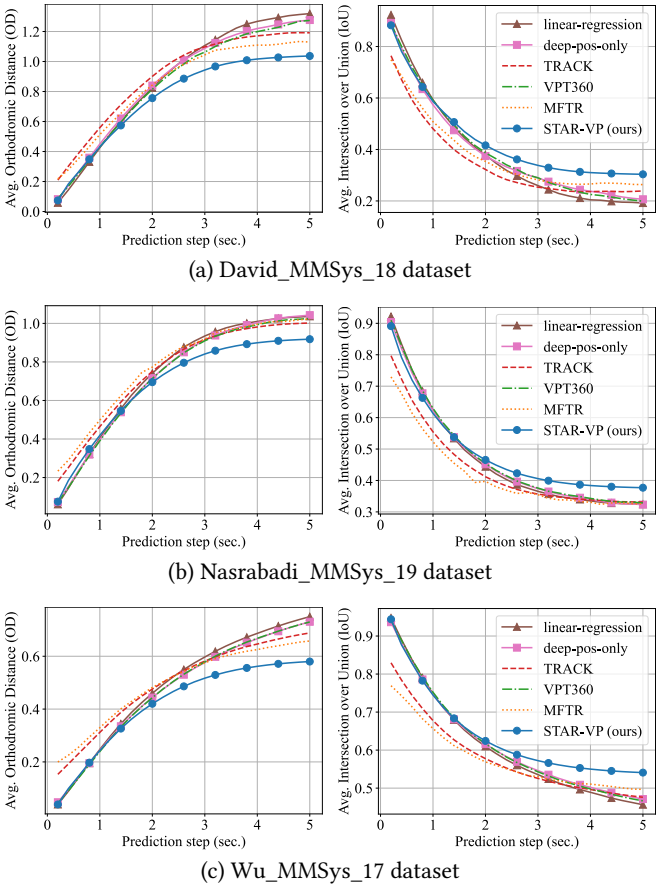

(a) David_MMSys_18 dataset

(b) Nasrabadi_MMSys_19 dataset

(c) Wu_MMSys_17 dataset

Figure 3: The Orthodromic Distance (OD) and Intersection over Union (IoU) against prediction steps of viewport prediction models on each dataset.

4.2 Results and Analysis

Fig. 3 shows the prediction performance of STAR-VP and five competitors on three datasets. From the figure, we can see that HT-only models (linear-regression, deep-pos-only, VPT360) have better performance in short-term prediction (<1s) as they are not influenced by VC information. The two competitors (TRACK, MFTR) that consider both HT and VC for prediction have better long-term prediction (2-5s) performance, but worse short-term prediction performance than HT-only models. This indicates that their improvement in long-term prediction performance comes at the expense of short-term prediction performance. In contrast, STAR-VP achieves the best long-term prediction performance without sacrificing short-term prediction performance. This is mainly due to the space-aligned and time-varying fusion of HT and VC by using $salxyz$ representation and the two-stage fusion method in STAR-VP. Table 2 further shows the average long-term prediction performance of each model on three datasets. We note that because TRACK and MFTR sacrifice short-term prediction performance to improve long-term prediction, their average performance over 2-5s is often worse than HT-only models such as deep-pos-only and

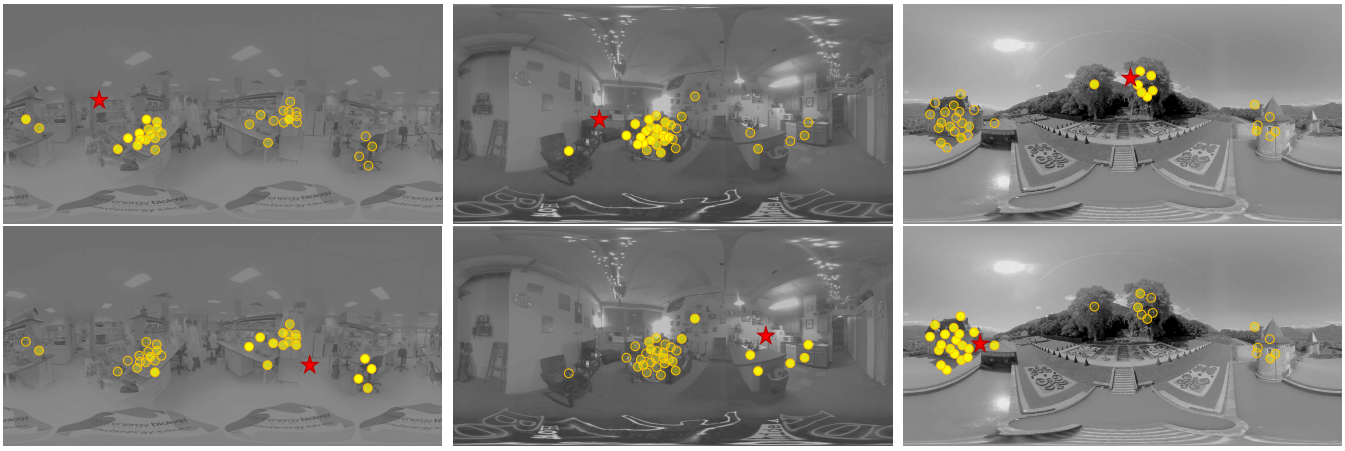

Figure 4: The visualization of the spatial attention scores assigned by STAR-VP to the saliency sampling points (yellow points) on three video frames, given two different user viewpoint positions (red star). The brighter the yellow point, the larger the spatial attention score.

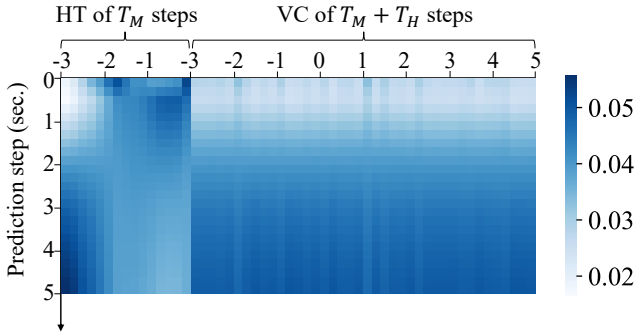

Figure 5: The heatmap of the column-normalized temporal attention scores between each prediction step and the HT/VC inputs from STAR-VP.

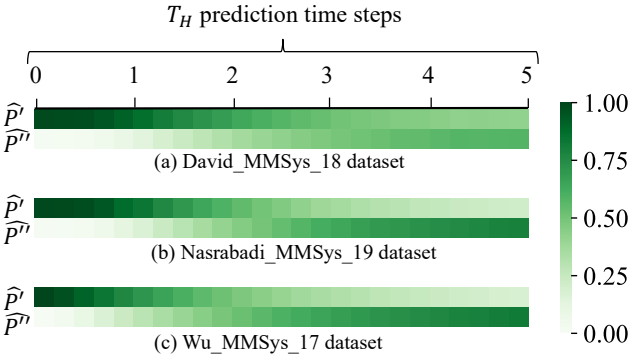

Figure 6: The heatmap of the weight allocation of the Gating Fusion Module in STAR-VP for $\widehat{P'}$ and $\widehat{P''}$ at each prediction time step on three datasets.

VPT360. Across all datasets and metrics, STAR-VP achieves state-of-the-art performance in long-term prediction and comparable performance in short-term prediction.

4.3 Visualization

4.3.1 Attention Scores of Spatial Attention Module. To analyze STAR-VP's ability to align HT and VC spatially, we multiply the attention matrices of its Spatial Attention Module to obtain the attention scores between the viewpoint and each saliency sampling point on video frames and visualize them as shown in Fig. 4. The figure shows how the attention scores of the saliency sampling points on three different video frames change with the spatial position of the current user viewpoint. The red star represents the current user's viewpoint on the video frame, and the yellow points are 32 points uniformly sampled from the *salxyz* representation of the current frame according to saliency value. The brighter the yellow point, the higher the attention score. It is evident from the figure that STAR-VP assigns higher attention scores to the saliency sampling points closer to the viewpoint. This indicates that it aligns the spatial information expressed by HT and VC well.

4.3.2 Attention Scores of Temporal Attention Module. To analyze the time-varying attention pattern of STAR-VP, we multiply the attention matrices of its Temporal Attention Module to obtain the attention scores between each prediction step and the HT/VC inputs, and visualize them as the heatmap shown in Fig. 5. It can be seen from the figure that as the prediction step increases, the attention scores of recent 2s HT gradually decrease, while the attention scores of VC and earlier HT gradually increase. This is consistent with the idea that HT reflects inertia for short-term viewpoint motion, while VC influences long-term motion through salient regions. We also observe that as the prediction step increases, STAR-VP gradually increases its attention to HT over the past 2s. This is because HT over the past 2s reflects certain user viewpoint motion preferences that are beneficial for long-term viewpoint prediction. In summary, the visualization results of the attention scores of

the Temporal Attention Module indicate that STAR-VP performs feature selection on HT and VC with a time-varying pattern in the first fusion stage. It is worth noting that to facilitate a clearer observation of the time-varying attention pattern, we apply min-max normalization to the original attention scores matrix along the columns.

4.3.3 Weight Allocation of Gating Fusion Module. We visualize the weight allocation of the Gating Fusion Module in STAR-VP for $\widehat{P'}$ and $\widehat{P''}$ at each prediction time step as a heatmap, as shown in Fig. 6. Here, $\widehat{P'}$ is the prediction result with better short-term performance output by the LSTM module that only considers HT, while $\widehat{P''}$ is the prediction result with better long-term performance output by the Temporal Attention Module after the first-stage fusion of HT and VC. It can be seen from the figure that for the initial prediction steps, the Gating Fusion Module almost assigns all the weight to $\widehat{P'}$. As the prediction step increases, the weight of $\widehat{P'}$ is gradually reduced, while that of $\widehat{P''}$ is increased. This allows STAR-VP to achieve excellent long-term prediction performance without sacrificing short-term performance.

4.4 Ablation Study

4.4.1 Effects of Each Module in STAR-VP. To analyze the contribution of each module in STAR-VP to the prediction performance, we conducted an ablation study on the Spatial Attention Module (SAM), Temporal Attention Module (TAM), and Gating Fusion Module (GFM). For SAM, we replaced it with a linear layer. For TAM, we replaced it with an LSTM. For GFM, we removed it directly and used the output of TAM as the final prediction result. The results are depicted in Fig. 7. It can be seen from the figure that removing any module will affect the prediction performance. Removing SAM and TAM mainly affects long-term prediction performance, while removing GFM mainly affects short-term performance. This result not only demonstrates the importance of each module but also indicates that the main role of SAM and TAM is to improve the long-term viewpoint prediction performance of STAR-VP, while the main role of GFM is to block the output of the long-term prediction module in short-term prediction to ensure the short-term viewpoint prediction performance of STAR-VP.

4.4.2 Effects of salxyz Representation. We tested the long-term prediction performance of three models that consider both HT and VC with the original saliency map and the *salxyz* representation,

Table 3: Ablation study results of *salxyz*: the long-term prediction (2-5s) performance of three models considering HT and VC with or without the *salxyz* representation. OD is Orthodromic Distance, and IoU is Intersection over Union.

	David_MMSys_18		Nasrabadi_MMSys_19		Wu_MMSys_17	
	OD ↓	IoU ↑	OD ↓	IoU ↑	OD ↓	IoU ↑
TRACK (w/o *salxyz*)	1.123	25.05%	0.939	35.05%	0.613	51.12%
TRACK (w/ *salxyz*)	1.144	24.62%	0.952	34.35%	0.626	50.90%
MFTR (w/o *salxyz*)	1.064	27.98%	0.954	34.27%	0.599	52.02%
MFTR (w/ *salxyz*)	1.123	27.34%	0.958	34.02%	0.613	52.03%
STAR-VP (w/o *salxyz*)	1.057	28.31%	0.928	36.91%	0.584	52.56%
STAR-VP (w/ *salxyz*)	**0.967**	**33.26%**	**0.862**	**39.84%**	**0.531**	**56.82%**

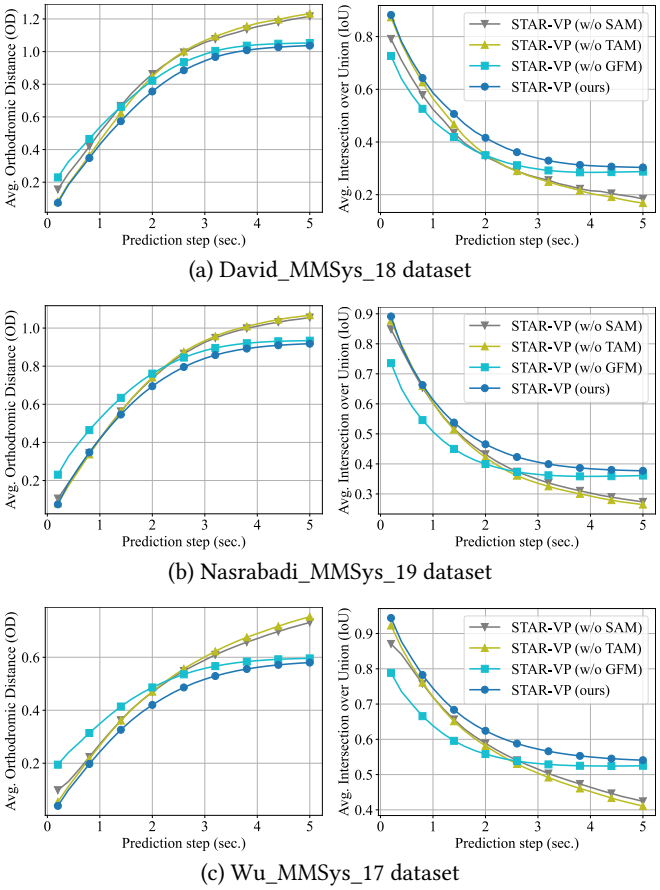

(a) David_MMSys_18 dataset

(b) Nasrabadi_MMSys_19 dataset

(c) Wu_MMSys_17 dataset

Figure 7: Ablation study results of Spatial Attention Module (SAM), Temporal Attention Module (TAM), and Gating Fusion Module (GFM) in STAR-VP on each dataset.

respectively. The results are shown in Table 3. From the test results, it can be seen that the performance of the TRACK and MFTR models decreases after using the *salxyz* representation, while only STAR-VP improves its performance after using the *salxyz* representation. This result demonstrates the improvement of the *salxyz* representation on long-term prediction performance and highlights the importance of the *salxyz* representation in conjunction with the Spatial Attention Module.

5 CONCLUSION

In this paper, we propose a novel long-term viewpoint prediction model STAR-VP. It fuses viewpoint and saliency information in a space-aligned and time-varying manner, achieving the best long-term prediction performance without sacrificing short-term prediction performance. A viewpoint prediction model with excellent long-term performance helps 360° video streaming systems predownload tiles for a longer time ahead, thereby establishing a longer buffer to cope with network fluctuations.

References

[1] Shahryar Afzal, Jiasi Chen, and KK Ramakrishnan. 2017. Characterization of 360-degree videos. In *Proceedings of the Workshop on Virtual Reality and Augmented Reality Network*. 1–6.

[2] Yixuan Ban, Lan Xie, Zhimin Xu, Xinggong Zhang, Zongming Guo, and Yue Wang. 2018. Cub360: Exploiting cross-users behaviors for viewport prediction in 360 video adaptive streaming. In *2018 IEEE International Conference on Multimedia and Expo (ICME)*. IEEE, 1–6.

[3] Nicolas Carion, Francisco Massa, Gabriel Synnaeve, Nicolas Usunier, Alexander Kirillov, and Sergey Zagoruyko. 2020. End-to-end object detection with transformers. In *European conference on computer vision*. Springer, 213–229.

[4] Fang-Yi Chao, Cagri Ozcinar, and Aljosa Smolic. 2021. Transformer-based Long-Term Viewport Prediction in 360° Video: Scanpath is All You Need.. In *MMSP*. 1–6.

[5] Jinyu Chen, Xianzhuo Luo, Miao Hu, Di Wu, and Yipeng Zhou. 2020. Sparkle: User-aware viewport prediction in 360-degree video streaming. *IEEE Transactions on Multimedia* 23 (2020), 3853–3866.

[6] Lovish Chopra, Sarthak Chakraborty, Abhijit Mondal, and Sandip Chakraborty. 2021. Parima: Viewport adaptive 360-degree video streaming. In *Proceedings of the Web Conference 2021*. 2379–2391.

[7] Junyoung Chung, Caglar Gulcehre, KyungHyun Cho, and Yoshua Bengio. 2014. Empirical evaluation of gated recurrent neural networks on sequence modeling. *arXiv preprint arXiv:1412.3555* (2014).

[8] Erwan J David, Jesús Gutiérrez, Antoine Coutrot, Matthieu Perreira Da Silva, and Patrick Le Callet. 2018. A dataset of head and eye movements for 360 videos. In *Proceedings of the 9th ACM Multimedia Systems Conference*. 432–437.

[9] Jacob Devlin, Ming-Wei Chang, Kenton Lee, and Kristina Toutanova. 2018. Bert: Pre-training of deep bidirectional transformers for language understanding. *arXiv preprint arXiv:1810.04805* (2018).

[10] Alexey Dosovitskiy, Lucas Beyer, Alexander Kolesnikov, Dirk Weissenborn, Xiaohua Zhai, Thomas Unterthiner, Mostafa Dehghani, Matthias Minderer, Georg Heigold, Sylvain Gelly, et al. 2020. An image is worth 16x16 words: Transformers for image recognition at scale. *arXiv preprint arXiv:2010.11929* (2020).

[11] Ching-Ling Fan, Jean Lee, Wen-Chih Lo, Chun-Ying Huang, Kuan-Ta Chen, and Cheng-Hsin Hsu. 2017. Fixation prediction for 360 video streaming in head-mounted virtual reality. In *Proceedings of the 27th Workshop on Network and Operating Systems Support for Digital Audio and Video*. 67–72.

[12] Xianglong Feng, Viswanathan Swaminathan, and Sheng Wei. 2019. Viewport prediction for live 360-degree mobile video streaming using user-content hybrid motion tracking. *Proceedings of the ACM on Interactive, Mobile, Wearable and Ubiquitous Technologies* 3, 2 (2019), 1–22.

[13] Dan Hendrycks and Kevin Gimpel. 2016. Gaussian error linear units (gelus). *arXiv preprint arXiv:1606.08415* (2016).

[14] Sepp Hochreiter and Jürgen Schmidhuber. 1997. Long short-term memory. *Neural computation* 9, 8 (1997), 1735–1780.

[15] Andrew Jaegle, Sebastian Borgeaud, Jean-Baptiste Alayrac, Carl Doersch, Catalin Ionescu, David Ding, Skanda Koppula, Daniel Zoran, Andrew Brock, Evan Shelhamer, et al. 2021. Perceiver io: A general architecture for structured inputs & outputs. *arXiv preprint arXiv:2107.14795* (2021).

[16] Yue Kang, Zhao Cai, Chee-Wee Tan, Qian Huang, and Hefu Liu. 2020. Natural language processing (NLP) in management research: A literature review. *Journal of Management Analytics* 7, 2 (2020), 139–172.

[17] Wonjae Kim, Bokyung Son, and Ildoo Kim. 2021. Vilt: Vision-and-language transformer without convolution or region supervision. In *International conference on machine learning*. PMLR, 5583–5594.

[18] Gen Li, Nan Duan, Yuejian Fang, Ming Gong, and Daxin Jiang. 2020. Unicoder-vl: A universal encoder for vision and language by cross-modal pre-training. In *Proceedings of the AAAI conference on artificial intelligence*, Vol. 34. 11336–11344.

[19] Junhua Liu, Boxiang Zhu, Fangxin Wang, Yili Jin, Wenyi Zhang, Zihan Xu, and Shuguang Cui. 2023. CaV3: Cache-assisted Viewport Adaptive Volumetric Video Streaming. In *2023 IEEE Conference Virtual Reality and 3D User Interfaces (VR)*. IEEE, 173–183.

[20] Ze Liu, Yutong Lin, Yue Cao, Han Hu, Yixuan Wei, Zheng Zhang, Stephen Lin, and Baining Guo. 2021. Swin transformer: Hierarchical vision transformer using shifted windows. In *Proceedings of the IEEE/CVF international conference on computer vision*. 10012–10022.

[21] Ze Liu, Jia Ning, Yue Cao, Yixuan Wei, Zheng Zhang, Stephen Lin, and Han Hu. 2022. Video swin transformer. In *Proceedings of the IEEE/CVF conference on computer vision and pattern recognition*. 3202–3211.

[22] Jiasen Lu, Dhruv Batra, Devi Parikh, and Stefan Lee. 2019. Vilbert: Pretraining task-agnostic visiolinguistic representations for vision-and-language tasks. *Advances in neural information processing systems* 32 (2019).

[23] Afshin Taghavi Nasrabadi, Aliehsan Samiei, Anahita Mahzari, Ryan P McMahan, Ravi Prakash, Mylène CQ Farias, and Marcelo M Carvalho. 2019. A taxonomy and dataset for 360 videos. In *Proceedings of the 10th ACM Multimedia Systems Conference*. 273–278.

[24] Afshin Taghavi Nasrabadi, Aliehsan Samiei, and Ravi Prakash. 2020. Viewport prediction for 360 videos: a clustering approach. In *Proceedings of the 30th ACM Workshop on Network and Operating Systems Support for Digital Audio and Video*. 34–39.

[25] Anh Nguyen, Zhisheng Yan, and Klara Nahrstedt. 2018. Your attention is unique: Detecting 360-degree video saliency in head-mounted display for head movement prediction. In *Proceedings of the 26th ACM international conference on Multimedia*. 1190–1198.

[26] Ozan Oktay, Jo Schlemper, Loic Le Folgoc, Matthew Lee, Mattias Heinrich, Kazunari Misawa, Kensaku Mori, Steven McDonagh, Nils Y Hammerla, Bernhard Kainz, et al. 2018. Attention u-net: Learning where to look for the pancreas. *arXiv preprint arXiv:1804.03999* (2018).

[27] Colin Raffel, Noam Shazeer, Adam Roberts, Katherine Lee, Sharan Narang, Michael Matena, Yanqi Zhou, Wei Li, and Peter J Liu. 2020. Exploring the limits of transfer learning with a unified text-to-text transformer. *Journal of machine learning research* 21, 140 (2020), 1–67.

[28] Miguel Fabián Romero Rondón, Lucile Sassatelli, Ramón Aparicio-Pardo, and Frédéric Precioso. 2020. A unified evaluation framework for head motion prediction methods in 360 videos. In *Proceedings of the 11th ACM Multimedia Systems Conference*. 279–284.

[29] Miguel Fabian Romero Rondon, Dario Zanca, Stefano Melacci, Marco Gori, and Lucile Sassatelli. 2021. Hemog: A white-box model to unveil the connection between saliency information and human head motion in virtual reality. In *2021 IEEE International Conference on Artificial Intelligence and Virtual Reality (AIVR)*. IEEE, 10–18.

[30] Miguel Fabián Romero Rondón, Lucile Sassatelli, Ramón Aparicio-Pardo, and Frédéric Precioso. 2022. TRACK: A New Method From a Re-Examination of Deep Architectures for Head Motion Prediction in 360 Videos. *IEEE Transactions on Pattern Analysis and Machine Intelligence* 44, 9 (2022), 5681–5699. https://doi.org/10.1109/TPAMI.2021.3070520

[31] Yingjie Song, Zhi Liu, Gongyang Li, Dan Zeng, Tianhong Zhang, Lihua Xu, and Jijun Wang. 2023. RINet: Relative Importance-Aware Network for Fixation Prediction. *IEEE Transactions on Multimedia* (2023).

[32] Ashish Vaswani, Noam Shazeer, Niki Parmar, Jakob Uszkoreit, Llion Jones, Aidan N Gomez, Łukasz Kaiser, and Illia Polosukhin. 2017. Attention is all you need. *Advances in neural information processing systems* 30 (2017).

[33] Mu Wang, Shuai Peng, Xingyan Chen, Yu Zhao, Mingwei Xu, and Changqiao Xu. 2022. CoLive: An Edge-Assisted Online Learning Framework for Viewport Prediction in 360° Live Streaming. In *2022 IEEE International Conference on Multimedia and Expo (ICME)*. IEEE, 1–6.

[34] Chenglei Wu, Zhihao Tan, Zhi Wang, and Shiqiang Yang. 2017. A dataset for exploring user behaviors in VR spherical video streaming. In *Proceedings of the 8th ACM on Multimedia Systems Conference*. 193–198.

[35] Lan Xie, Zhimin Xu, Yixuan Ban, Xinggong Zhang, and Zongming Guo. 2017. 360probdash: Improving qoe of 360 video streaming using tile-based http adaptive streaming. In *Proceedings of the 25th ACM international conference on Multimedia*. 315–323.

[36] Yanyu Xu, Yanbing Dong, Junru Wu, Zhengzhong Sun, Zhiru Shi, Jingyi Yu, and Shenghua Gao. 2018. Gaze prediction in dynamic 360 immersive videos. In *proceedings of the IEEE Conference on Computer Vision and Pattern Recognition*. 5333–5342.

[37] Yanyu Xu, Ziheng Zhang, and Shenghua Gao. 2021. Spherical DNNs and Their Applications in 360° Images and Videos. *IEEE Transactions on Pattern Analysis and Machine Intelligence* 44, 10 (2021), 7235–7252.

[38] Heeseung Yun, Sehun Lee, and Gunhee Kim. 2022. Panoramic Vision Transformer for Saliency Detection in 360 Videos. In *European Conference on Computer Vision*. Springer, 422–439.

[39] Xue Zhang, Gene Cheung, Patrick Le Callet, and Jack ZG Tan. 2020. Sparse directed graph learning for head movement prediction in 360 video streaming. In *ICASSP 2020-2020 IEEE International Conference on Acoustics, Speech and Signal Processing (ICASSP)*. IEEE, 2678–2682.

[40] Xue Zhang, Gene Cheung, Yao Zhao, Patrick Le Callet, Chunyu Lin, and Jack ZG Tan. 2021. Graph learning based head movement prediction for interactive 360 video streaming. *IEEE Transactions on Image Processing* 30 (2021), 4622–4636.

[41] Zhiahao Zhang, Yiwei Chen, Weizhan Zhang, Caixia Yan, Qinghua Zheng, Qi Wang, and Wangdu Chen. 2023. Tile Classification Based Viewport Prediction with Multi-modal Fusion Transformer. In *Proceedings of the 31st ACM International Conference on Multimedia*. 3560–3568.

[42] Ziheng Zhang, Yanyu Xu, Jingyi Yu, and Shenghua Gao. 2018. Saliency detection in 360 videos. In *Proceedings of the European conference on computer vision (ECCV)*. 488–503.

[43] Pengyu Zhao, Yuanxing Zhang, Kaigui Bian, Hu Tuo, and Lingyang Song. 2019. Laddernet: Knowledge transfer based viewpoint prediction in 360○ video. In *ICASSP 2019-2019 IEEE International Conference on Acoustics, Speech and Signal Processing (ICASSP)*. IEEE, 1657–1661.

[44] Xiaoqi Zhao, Youwei Pang, Lihe Zhang, Huchuan Lu, and Lei Zhang. 2020. Suppress and balance: A simple gated network for salient object detection. In *Computer Vision–ECCV 2020: 16th European Conference, Glasgow, UK, August 23–28, 2020, Proceedings, Part II 16*. Springer, 35–51.